Supplementary Information

Structurally Stable Mg-doped P2-$Na_{2/3}Mn_{1-y}Mg_yO_2$ Sodium-ion Battery Cathodes with High Rate Performance: Insights from Electrochemical, NMR and Diffraction Studies

Raphaële J. Clément,[a] Juliette Billaud,[b] A. Robert Armstrong,[b] Gurpreet Singh,[c] Teófilo Rojo,[c] Peter G. Bruce,[b,d] Clare P. Grey[a]

[a]Department of Chemistry, University of Cambridge, Cambridge CB2 1EW, United Kingdom

[b]School of Chemistry, University of St. Andrews, St. Andrews, Fife KY16 9ST, United Kingdom

[c]CIC ENERGIGUNE, Parque Tecnológico de Álava, Albert Einstein 48, ED. CIC, 01510 Miñano, Spain

[d]Department of Materials, University of Oxford, Oxford OX1 3PH, United Kingdom

I. Additional electrochemical data

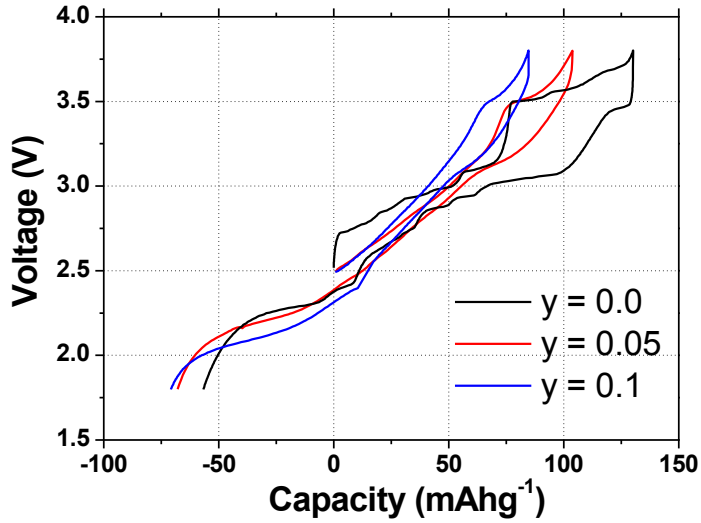

Figure S1. First cycle electrochemical profiles of the $Na_{2/3}Mn_{1-y}Mg_yO_2$ (y = 0.0, 0.05 and 0.1) compositions. The compounds were cycled at 10 mAg^{-1} between 1.8 and 3.8 V vs. Na^+/Na.

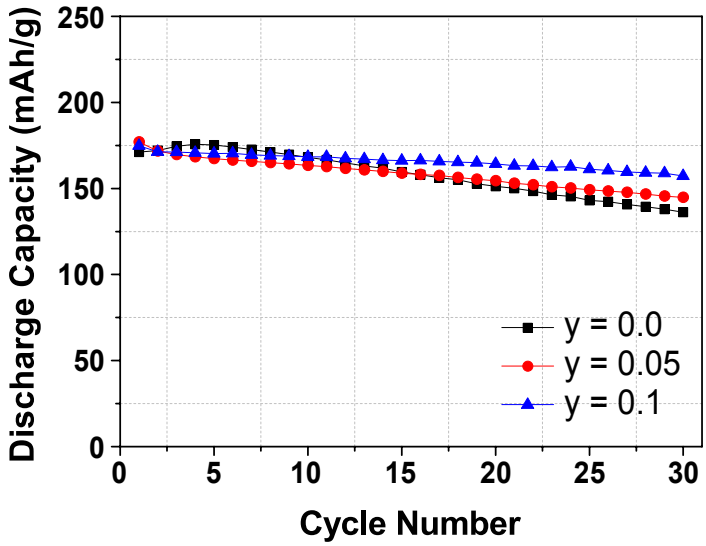

Figure S2. Evolution of the discharge capacity as a function of the cycle number for $Na_{2/3}Mn_{1-y}Mg_yO_2$ (y = 0.0, 0.05, and 0.1). The cells were cycled between 1.5 and 4.0 V vs. Na^+/Na, and charged and discharged at 12 mAg^{-1}.

II. Fitted diffraction patterns and crystallographic parameters

1. Na_xMnO_2

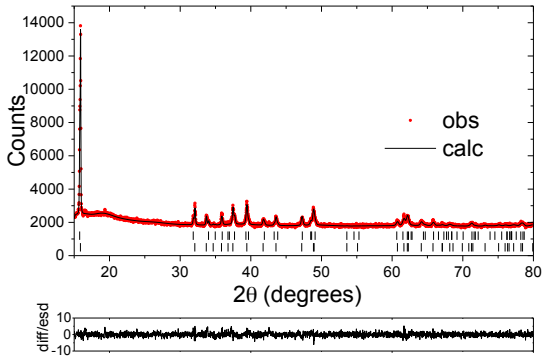

Figure S3. Fitted powder XRD pattern for the as-prepared $Na_{2/3}MnO_2$ compound. In this and all subsequent diffraction patterns, the red dots represent the observed data, and the solid line the calculated pattern; the lower line is the difference/esd. Tick marks represent the allowed reflections. Phase 1 (lower tick marks) corresponds to the orthorhombic $Na_{2/3}MnO_2$ phase (*Cmcm*) and phase 2 (upper tick marks) relates to the monoclinic $Na_{2/3}MnO_2$ phase (*C*2/*n*).

Table S1. Refined parameters of the $Na_{2/3}MnO_2$ compound. R_{wp} = 2.67 %, R_e = 2.22 %, R_p = 2.09 %. In this and all subsequent tables, the e and f labels indicate edge- and face-centered sites, respectively.

70 % Orthorhombic phase *(Cmcm)*						
Atom	**Wyckoff**	***x*/a**	***y*/b**	***z*/c**	**Occupancy**	**B_{iso}**
Na1(e)	4c	0	0.331(5)	0.25	0.44(1)	1
Na2(f)	4c	0	0.068(11)	0.25	0.22(1)	1
Mn1	4a	0	0	0	1	0.1(2)
O1	8f	0	0.641(2)	0.0794(8)	1	0.9
a = 2.8368(2) Å, *b* = 5.3153(4) Å, *c* = 11.1538(12) Å						
30 % Monoclinic phase (*C*2/*n*)						
Atom	**Wyckoff**	***x*/a**	***y*/b**	***z*/c**	**Occupancy**	**B_{iso}**
Na1(e)	4e	0	0.299(10)	0.25	0.43(3)	1
Na2(f)	4e	0	0	0.25	0.22(3)	1
Mn1	4a	0	0	0	1	0.6
O1	8f	0.004(6)	0.632(4)	0.086(2)	1	0.9
a = 2.8342(7) Å, *b* = 5.2669(8) Å, *c* = 11.2304(13) Å and β = 90.78(2)						

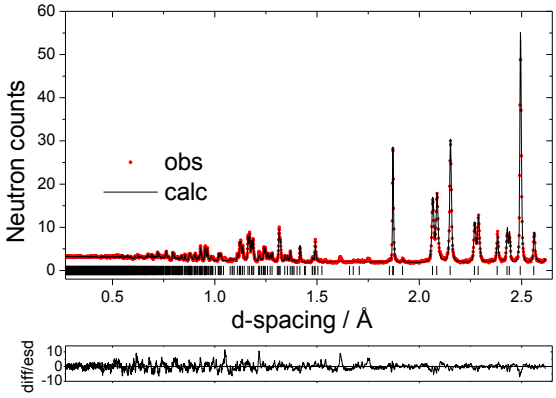

Figure S4. Fitted powder neutron diffraction pattern for the as-prepared $Na_{0.62}MnO_2$ compound.

Table S2. a) Refined crystallographic parameters for $Na_{0.62}MnO_2$ in the *C*2/*n* space group, *a* = 2.83245(8) Å, *b* = 5.2580(2) Å, *c* = 11.2195(3) Å, *β* =90.701(3). R_{wp} = 3.85 %, R_e = 1.65 %, R_p = 3.80 %.

$Na_{0.62}MnO_2$ (*C*2/*n*)						
Atom	**Wyckoff**	***x*/a**	***y*/b**	***z*/c**	**Occupancy**	**B_{iso}**
Na1(e)	4e	0	0.325(2)	0.25	0.46(2)	1.96(13)
Na2(f)	4e	0	-0.079(3)	0.25	0.19(1)	1.96(13)
Mn1	4a	0	0	0	1	0.09(2)
O1	8f	0.0044(6)	0.6489(3)	0.0923(2)	1	0.82(2)
a = 2.83245(8) Å, *b* = 5.2580(2) Å, *c* = 11.2195(3) Å, *β* =90.701(3)						

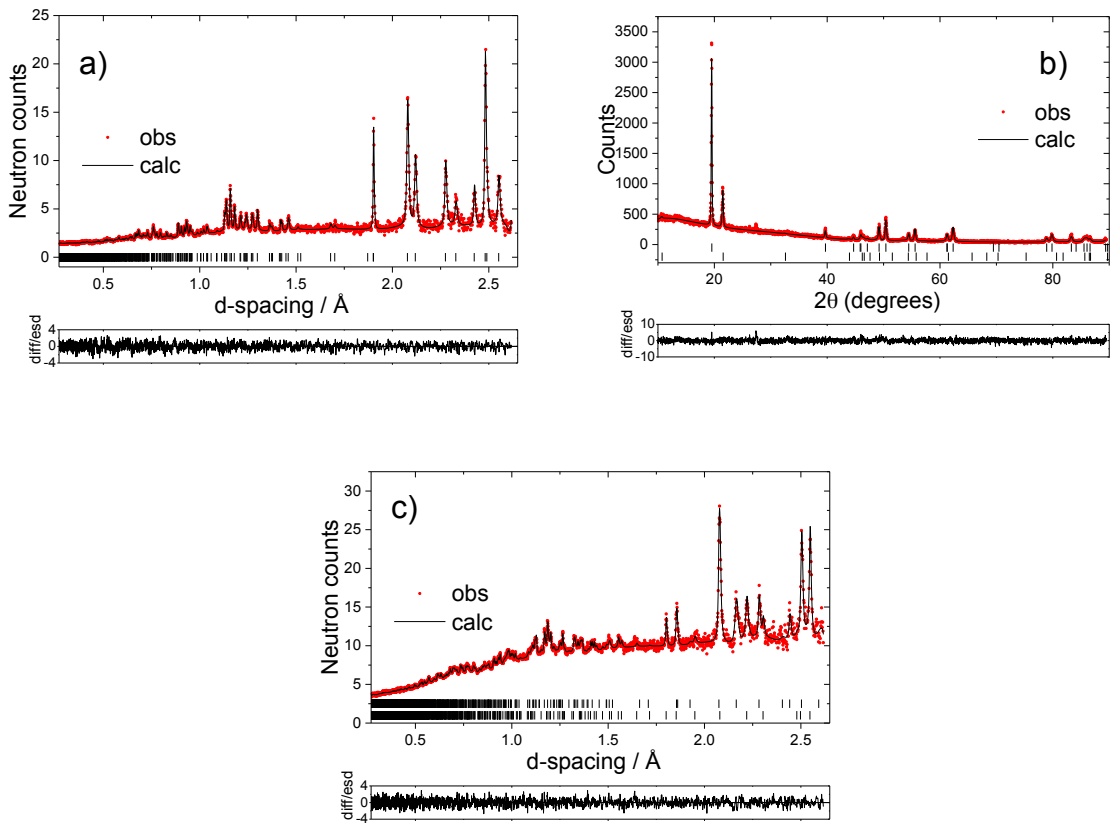

Figure S5. Fitted powder diffraction patterns for: a) $Na_{0.37}MnO_2$ following charging to 3.5 V (neutron data); b) $Na_{0.31}MnO_2$ formed after the extended plateau at the end of charge (XRD data; upper tick marks correspond to the orthorhombic phase (*Cmcm*) and lower tick marks to the OP4 phase); and c) $Na_{0.82}MnO_2$ obtained at the end of discharge (neutron data; lower tick marks correspond to the orthorhombic Na_1MnO_2 phase and upper tick marks to the $Na_{2/3}MnO_2$ phase).

Table S3. Refined crystallographic parameters for: a) $Na_{0.37}MnO_2$ in the *Cmcm* space group (R_{wp} = 4.13%, R_e = 4.63%, R_p = 4.39%); b) $Na_{0.31}MnO_2$ (R_{wp} = 8.71%, R_e = 7.92%, R_p = 6.43%); and c) $Na_{0.82}MnO_2$ (R_{wp} = 1.98%, R_e = 2.23%, R_p = 2.26%).

a) $Na_{0.37}MnO_2$ (*Cmcm*)						
Atom	**Wyckoff**	***x*/a**	***y*/b**	***z*/c**	**Occupancy**	**B_{iso}**
Na1(e)	4c	0	0.325(3)	0.25	0.29(2)	0.8(3)
Na2(f)	4c	0	0	0.25	0.046(11)	1
Mn1	4a	0	0	0	1	0.28(4)
O1	8f	0	0.6592(5)	0.0865(2)	1	1
a = 2.8395(1) Å, b = 5.1029(4) Å, c = 11.4055(5) Å, β = 90.701(3)						

b) $Na_{0.31}MnO_2$

66% Orthorhombic phase (*Cmcm*)

Atom	Wyckoff	*x*/a	*y*/b	*z*/c	Occupancy	B_{iso}
Na1(e)	4c	0	0.325(3)	0.25	0.45(2)	2.6(12)
Na2(f)	4c	0	0	0.25	0.039(8)	1
Mn1	4a	0	0	0	1	0.8(2)
O1	8f	0	0.6593(13)	0.0922(6)	1	1
a = 2.8371(2) Å, *b* = 5.0929(4) Å, *c* = 11.4049(12) Å						

34 % OP4 phase ($P6_3/mmc$)

Atom	Wyckoff	*x*/a	*y*/b	*z*/c	Occupancy	B_{iso}
Na1(e)	2c	0.3333	0.6667	0.25	0.58(5)	2
Mn1	4f	0.6667	0.3333	0.3842(13)	1	0.6
O1	4f	0.3333	0.6667	0.4482(13)	1	1
O2	4e	0	0	0.3340(16)	1	1
a = 2.847(4) Å, *c* = 20.695(6) Å						

c) $Na_{0.82}MnO_2$

44 % Na_1MnO_2 phase (*Cmcm*)

Atom	Wyckoff	*x*/a	*y*/b	*z*/c	Occupancy	B_{iso}
Na1(e)	4c	0	0.2998(14)	0.25	1	0.49(10)
Mn1	4a	0	0	0	1	0.46(7)
O1	8f	0	0.6251(6)	0.1012 (3)	1	0.19(3)
a = 2.8556(3) Å, *b* = 5.6338(8) Å, *c* = 10.8064(13) Å						

56% $Na_{2/3}MnO_2$ (*Cmcm*)

Atom	Wyckoff	*x*/a	*y*/b	*z*/c	Occupancy	B_{iso}
Na1(e)	4c	0	0.326(2)	0.25	0.48(5)	0.7(3)
Na2(f)	4c	0	0	0.25	0.14(3)	1
Mn1	4a	0	0	0	1	0.77(12)
O1	8f	0	0.6451(8)	0.0963(3)	1	0.65(6)
a = 2.8350(3) Å, *b* = 5.3319(8) Å, *c* = 11.1292(14) Å						

2. $Na_xMn_{0.95}Mg_{0.05}O_2$

Table S4. Refined crystallographic parameters for: a) $Na_{0.38}Mn_{0.95}Mg_{0.05}O_2$ in the *Cmcm* space group (R_{wp} = 3.12%, R_e = 3.31%, R_p = 3.30%); b) $Na_{0.28}Mn_{0.95}Mg_{0.05}O_2$ (R_{wp} = 4.18%, R_e = 4.63%, R_p = 4.29%); c) $Na_{0.92}Mn_{0.95}Mg_{0.05}O_2$ (R_{wp} = 2.29%, R_e = 2.50%, R_p = 2.52%).

a) $Na_{0.38}Mn_{0.95}Mg_{0.05}O_2$ (*Cmcm*)						
Atom	**Wyckoff**	***x*/a**	***y*/b**	***z*/c**	**Occupancy**	**B_{iso}**
Na1(e)	4c	0	0.343(8)	0.25	0.33(2)	0.7(4)
Mn1/Mg1	4a	0	0	0	0.948(9)/0.052	0.05(5)
O1	8f	0	0.6663(10)	0.0867(2)	1	0.69(4)
a = 2.8528(3) Å, *b* = 5.0325(14) Å, *c* = 11.3625(15) Å						

b) $Na_{0.28}Mn_{0.95}Mg_{0.05}O_2$						
60 % P2 phase ($P6_3/mmc$)						
Atom	**Wyckoff**	***x*/a**	***y*/b**	***z*/c**	**Occupancy**	**B_{iso}**
Na1(f)	2b	0	0	0.25	0.15	1
Na2(e)	2d	0.6667	0.3333	0.25	0.2	1
Mn1/Mg1	2a	0	0	0.5	0.95/0.05	0.6
O1	4e	0.3333	0.6667	0.0856(5)	1	0.7
a = 2.863(2) Å, *c* = 11.087(7) Å						
40 % OP4 phase ($P6_3/mmc$)						
Atom	**Wyckoff**	***x*/a**	***y*/b**	***z*/c**	**Occupancy**	**B_{iso}**
Na1(e)	2c	0.3333	0.6667	0.25	0.24(5)	2
Mn1/Mg1	4f	0.6667	0.3333	0.3921(15)	0.95/0.05	0.6
O1	4f	0.3333	0.6667	0.4296(8)	1	1
O2	4e	0	0	0.3376(7)	1	1
a = 2.8491(3) Å, *c* = 20.969(10) Å						

c) $Na_{0.92}Mn_{0.95}Mg_{0.05}O_2$						
78% Orthorhombic phase (*Cmcm*)						
Atom	**Wyckoff**	***x*/a**	***y*/b**	***z*/c**	**Occupancy**	**B_{iso}**
Na1(e)	4c	0	0.3084(8)	0.25	0.93(3)	0.36(6)
Mn1/Mg1	4a	0	0	0	0.953(8)/0.047	0.31(6)
O1	8f	0	0.6294(5)	0.1010(2)	1	0.38(3)
a = 2.8643(3) Å, *b* = 5.5738(11) Å, *c* = 10.8064(11) Å						
22% Orthorhombic phase (*Cmcm*)						
Atom	**Wyckoff**	***x*/a**	***y*/b**	***z*/c**	**Occupancy**	**B_{iso}**
Na1(e)	4c	0	0.332(5)	0.25	0.80(12)	0.1(3)
Mn1/Mg1	4a	0	0	0	0.95/0.05	0.3(2)
O1	8f	0	0.650(3)	0.1028(7)	1	0.7
a = 2.8756(12) Å, *b* = 5.361(5) Å, *c* = 11.000(6) Å						

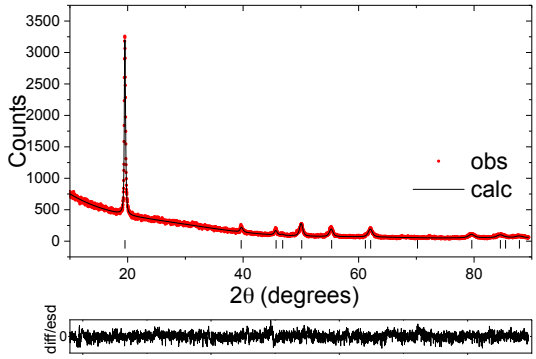

Figure S6. Fitted powder XRD pattern for the $Na_{0.40}Mn_{0.95}Mg_{0.05}O_2$ phase formed on discharge.

Table S5. Refined parameters for $Na_{0.40}Mn_{0.95}Mg_{0.05}O_2$ in the $P6_3/mmc$ space group. R_{wp} = 7.41 %, R_e = 6.96 %, R_p = 3.37 %.

$Na_{0.40}Mn_{0.95}Mg_{0.05}O_2$ ($P6_3/mmc$)						
Atom	**Wyckoff**	***x*/a**	***y*/b**	***z*/c**	**Occupancy**	**B_{iso}**
Na1(e)	2d	0.6667	0.3333	0.25	0.36(5)	1.3
Na2(f)	2a	0	0	0.25	0.03(3)	1.3
Mn1/Mg1	2a	0	0	0.5	0.95/0.05	0.5
O2	4e	0.3333	0.6667	0.084(3)	1	0.7
a = 2.8782(11) Å, c = 11.413(9) Å						

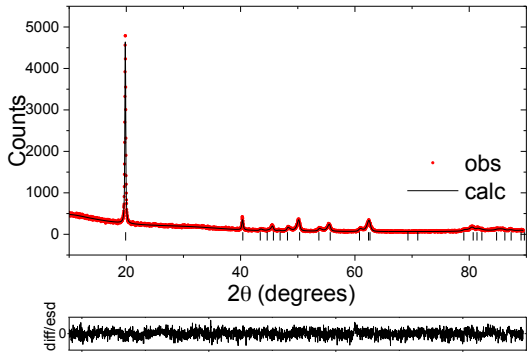

Figure S7. Fitted powder XRD pattern for the $Na_{0.60}Mn_{0.95}Mg_{0.05}O_2$ phase formed on discharge.

Table S6. Refined parameters for $Na_{0.60}Mn_{0.95}Mg_{0.05}O_2$ in the *Cmcm* space group. R_{wp} = 7.87 %, R_e = 7.56 %, R_p = 5.91 %.

$Na_{0.60}Mn_{0.95}Mg_{0.05}O_2$ (*Cmcm*)						
Atom	**Wyckoff**	***x*/a**	***y*/b**	***z*/c**	**Occupancy**	**B_{iso}**
Na1(e)	4c	0	0.318(3)	0.25	0.399(9)	1.3
Na2(f)	4c	0	0	0.25	0.232(7)	1.3
Mn1/Mg1	4a	0	0	0	0.95/0.05	0.5
O1	8f	0	0.643(3)	0.0938(11)	1	0.7
a = 2.8325(5) Å, *b* = 5.2327(14) Å, *c* = 11.214(3) Å						

3. $Na_xMn_{0.9}Mg_{0.1}O_2$

Table S7. a) Refined crystallographic parameters for: a) $Na_{0.40}Mn_{0.9}Mg_{0.1}O_2$ in the *P6₃/mmc* space group (R_{wp} = 6.21%, R_e = 2.92%, R_p = 4.64%); b) $Na_{0.32}Mn_{0.9}Mg_{0.1}O_2$ (R_{wp} = 8.56%, R_e = 3.70%, R_p = 6.40%); and c) $Na_{0.98}Mn_{0.9}Mg_{0.1}O_2$ (R_{wp} = 8.13%, R_e = 2.45%, R_p = 6.16%).

a) $Na_{0.40}Mn_{0.9}Mg_{0.1}O_2$ *(P6₃/mmc)*						
Atom	**Wyckoff**	***x*/a**	***y*/b**	***z*/c**	**Occupancy**	**B_{iso}**
Na1(f)	2b	0	0	0.25	0.09(1)	8.1(16)
Na2(e)	2d	0.6667	0.3333	0.25	0.332(9)	4.3(3)
Mn1/Mg1	2a	0	0	0.5	0.889(9)/0.111	0.59(1)
O1	4e	0.3333	0.6667	0.0878(2)	1	0.81(6)
a = 2.8801(4) Å, *c* = 11.396(3) Å						

b) $Na_{0.32}Mn_{0.9}Mg_{0.1}O_2$						
65 % P2 phase (*P6₃/mmc*)						
Atom	**Wyckoff**	***x*/a**	***y*/b**	***z*/c**	**Occupancy**	**B_{iso}**
Na1(f)	2b	0	0	0.25	0.169(9)	1
Na2(e)	2d	0.6667	0.3333	0.25	0.244(9)	1
Mn1/Mg1	2a	0	0	0.5	0.9/0.1	0.18(3)
O1	4e	0.3333	0.6667	0.0884(8)	1	0.80(11)
a = 2.8589(3) Å, *c* = 11.3898(13) Å						
35 % OP4 phase (*P6₃/mmc*)						
Atom	**Wyckoff**	***x*/a**	***y*/b**	***z*/c**	**Occupancy**	**B_{iso}**
Na1(e)	2c	0.3333	0.6667	0.25	0.33	2
Mn1/Mg1	4f	0.6667	0.3333	0.3841(2)	0.9/0.1	0.6
O1	4f	0.3333	0.6667	0.4165(7)	1	1
O2	4e	0	0	0.3365(7)	1	1
a = 2.8561(10) Å, *c* = 21.523(13) Å						

c) $Na_{0.98}Mn_{0.9}Mg_{0.1}O_2$						
88% Orthorhombic phase (*Cmcm*)						
Atom	**Wyckoff**	***x*/a**	***y*/b**	***z*/c**	**Occupancy**	**B_{iso}**
Na1(e)	4c	0	0.2961(5)	0.25	1	1
Mn1/Mg1	4a	0	0	0	0.9/0.1	0.5
O1	8f	0	0.6266(6)	0.1000(3)	1	0.7
a = 2.8693(2) Å, *b* = 5.5450(3) Å, *c* = 10.7879(5) Å						
12 % Orthorhombic phase (*Cmcm*)						
Atom	**Wyckoff**	***x*/a**	***y*/b**	***z*/c**	**Occupancy**	**B_{iso}**
Na1(e)	4c	0	0.315(4)	0.25	0.87(3)	1
Na2(f)	4c	0	0	0.25	0.07(2)	1
Mn1/Mg1	4a	0	0	0	0.9/0.1	0.5
O1	8f	0	0.648(4)	0.081(2)	1	0.7
a = 2.8784(2) Å, *b* = 5.3155(2) Å, *c* = 10.998(1) Å						

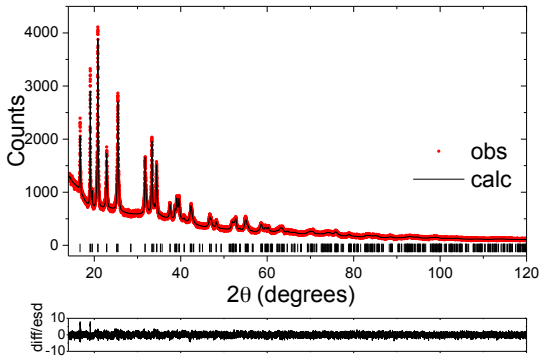

Figure S8. Fitted synchrotron diffraction pattern for the $Na_{0.43}Mn_{0.9}Mg_{0.1}O_2$ phase formed on discharge.

Table S8. Refined parameters for the $Na_{0.43}Mn_{0.9}Mg_{0.1}O_2$ compound in the *Cmcm* space group. R_{wp} = 5.01 %, R_e = 2.45 %, R_p = 3.85 %.

$Na_{0.43}Mn_{0.9}Mg_{0.1}O_2$ (*Cmcm*)						
Atom	**Wyckoff**	***x*/a**	***y*/b**	***z*/c**	**Occupancy**	**B_{iso}**
Na1(e)	4c	0	0.348(4)	0.25	0.268(8)	2.5(3)
Na2(f)	4c	0	0.973(8)	0.25	0.122(10)	1.9(7)
Mn1/Mg1	4a	0	0	0	0.916(11)/0.084	0.36(1)
O1	8f	0	0.6545(13)	0.0886(3)	1	0.66(6)
a = 2.8746(3) Å, *b* = 5.0029(3) Å, *c* = 11.3861(7) Å						

III. NMR

1. Rationalization of the evolution of the main ^{23}Na resonance upon Na deintercalation from P2-Na_xMnO_2

An abrupt decrease in the average ^{23}Na resonance, concurrent with partial layer shearing and the formation of an OP4 phase, is observed in Na_xMnO_2 between x = 0.31 and x = 0.23 (see Figure 5 in the main text). While both octahedral and prismatic sites are present in the OP4 phase, the electrostatic energy is minimized when all Na^+ ions occupy prismatic sites.[1] In fact, refined crystallographic parameters for $Na_{0.31}MnO_2$ (Table S3b) indicate that only edge-centered prismatic (P(2d)) sites are occupied in the OP4 phase. The broad high voltage ^{23}Na NMR signal at 1100 ppm is therefore assigned to P(2d) Na environments, an example of which is depicted in Figure S9.

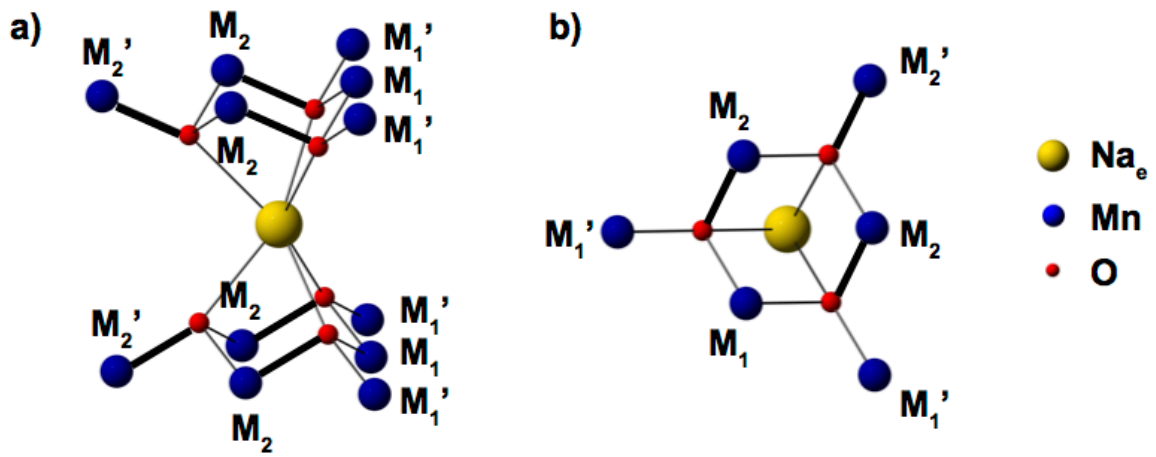

Figure S9. An ideal (undistorted) edge-centered prismatic Na site: a) viewed side on, and b) viewed from above. M_1, M_2 and M_1', M_2' correspond to inequivalent Mn sites in the first (M) and second (M') coordination shell of the Na^+ ion. Jahn-Teller elongated Mn-O bonds are depicted in bold.

In the OP4 phase, Na^+ ions occupy highly distorted P(2d) sites: the Mn atoms are drawn away from the empty octahedral Na layers, towards the occupied prismatic layers, resulting in shorter Na-Mn and O-Mn bonds, for all Mn atoms in the first (M) and in the second (M') coordination shells around the edge-centered Na site. Upon layer shearing, the Na-O-Mn bond angle increases (i.e. it deviates further from 90°) for Mn in the first coordination shell, while it decreases for Mn atoms in the second coordination shell (i.e. it deviates further from 180°). Since the ^{23}Na Fermi contact NMR shift strongly depends on the geometry of the Na-O-Mn spin density transfer pathways, such structural changes likely contribute to the decrease in the Na resonant frequency and the appearance of the broad 1100 ppm peak upon layer shearing ($x \leq 0.31$).

In addition, first principles ^{23}Na NMR parameters computed in the α-NaMn(III)O_2 and P2-$Na_{2/3}Ni_{1/3}Mn(IV)_{2/3}O_2$ structures (the subject of future publications) suggest that the oxidation of Mn in position M_2' relative to the central Na (see Figure S9) leads to a > 300 ppm reduction in the net ^{23}Na shift. On the other hand, the oxidation of Mn in M_1, M_1', and M_2 positions is expected to increase the total ^{23}Na shift. The late oxidation of Mn ions in M_2' positions would allow the favorable interlayer 180° Mn^{3+}-O-A-O-Mn^{3+} (A = Li^+, Na^+) interactions, reported in previous studies on layered mixed valence alkali manganese oxides,[2,3] to be maintained for as long as possible upon charge. In light of this, the following scenario may be put forward: Mn ions in M_1, M_2, and M_1' positions are oxidized at the beginning of charge and lead to an increase in the net Na shift, Mn ions in M_2' sites are oxidized at the end of charge and, together with changes in the local geometry around P(2d) Na sites, lead to a reduction in the net Na shift.

2. Composition of the as-synthesized $Na_{2/3}Mn_{1-y}Mg_yO_2$ samples (y = 0.05, 0.1)

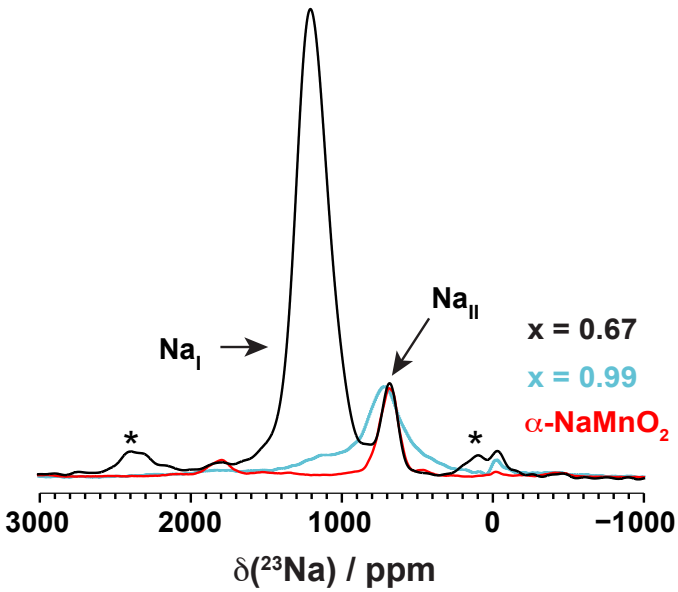

Figure S10. Comparison of the ^{23}Na solid-state MAS NMR spectra obtained for the as-synthesized $Na_{0.67}Mn_{0.95}Mg_{0.05}O_2$ phase, for the reduced $Na_{0.99}Mn_{0.95}Mg_{0.05}O_2$ phase, and for an O3' α-$NaMnO_2$ sample after air exposure. The peak near 0 ppm is most probably due to residual Na_2CO_3 precursor. The asterisks (*) indicate the spinning sidebands of the main ^{23}Na NMR resonances introduced by fast rotation of the sample (MAS).

Figure S10 compares the ^{23}Na NMR spectrum of the as-synthesized $Na_{0.67}Mn_{0.95}Mg_{0.05}O_2$ phase with that of the reduced $Na_{0.99}Mn_{0.95}Mg_{0.05}O_2$ phase and that of an O3' α-$NaMnO_2$ sample exposed to air. α-$NaMnO_2$ is highly air sensitive, yet for the sake of comparison it was handled in air in a similar way as the as-synthesized $Na_{0.67}Mn_{0.95}Mg_{0.05}O_2$ compound (the latter is not prone to air oxidation). The above spectra clearly show that the secondary (Na_{II}) peak observed in $Na_{0.67}Mn_{0.95}Mg_{0.05}O_2$ does not correspond to a minor reduced phase (e.g. $Na_{0.99}Mn_{0.95}Mg_{0.05}O_2$), but it arises from the presence of an impurity $NaMnO_2$ phase in the starting material. This impurity phase quickly undergoes oxidation, as indicated by the perfect overlap with the ^{23}Na spectrum of the oxidized α-$NaMnO_2$ phase, with peaks at ca. 700 and 1800 ppm.

References

1. C. Delmas, C. Fouassier, and P. Hagenmuller, *Physica B+C*, 1980, **99**, 81–85.
2. X. Li, X. Ma, D. Su, L. Liu, R. Chisnell, S. P. Ong, H. Chen, A. Toumar, J.-C. Idrobo, Y. Lei, J. Bai, F. Wang, J. W. Lynn, Y. S. Lee, and G. Ceder, *Nat. Mater.*, 2014, **13**, 586–592.
3. M. E. Arroyo y de Dompablo, C. Marianetti, A. Van der Ven, and G. Ceder, *Phys. Rev. B*, 2001, **63**, 144107.